Oxygen tri-clusters make glass highly crack-resistant

Shan, Z.T.; Zhao, T.Y.; Ke, X.F.; Ren, J.J.; Tao, H.Z.; Yue, Yuanzheng

Published in:
Acta Materialia

DOI (link to publication from Publisher):
10.1016/j.actamat.2023.119425

Publication date:
2024

Document Version
Accepted author manuscript, peer reviewed version

Oxygen tri-clusters make glass highly crack-resistant

Zhitao Shan[1,4], Tongyao Zhao[2,4], Xuefei Ke[1,4], Jinjun Ren[2]*, Haizheng Tao[1]*, Yuanzheng Yue[3]*

[1]State Key Laboratory of Silicate Materials for Architectures, Wuhan University of Technology, Wuhan 430070, China

[2]Key Laboratory of Materials for High-Power Laser, Shanghai Institute of Optics and Fine Mechanics, Chinese Academy of Sciences, Shanghai 201800, China

[3]Department of Chemistry and Bioscience, Aalborg University, DK-9220 Aalborg, Denmark

[4]These authors contributed equally: Zhitao Shan, Tongyao Zhao, Xuefei Ke.

*Corresponding authors: jinjunren@siom.ac.cn; thz@whut.edu.cn; yy@bio.aau.dk

Abstract: Identifying key structural factors that surmount their intrinsic brittleness and poor crack initiation resistance (C_R) is crucial for designing glass efficiently and predictably. In this study, we present three significant discoveries that contribute to the design of glasses with superior mechanical performances. Firstly, the C_R of the aluminosilicate glasses exhibited a drastic increase when the alumina content surpasses a critical threshold. Secondly, the fraction of three-coordinated oxygens (i.e., oxygen tri-cluster fraction [$^{(3)}$O]) was successfully quantified using our new Nuclear Magnetic Resonance technique. Thirdly, a remarkable correlation between the evolution trend of the [$^{(3)}$O] and the alumina content was established, which aligns closely with the C_R trend. These findings suggest that oxygen tri-clusters play a crucial role in significantly enhancing C_R in aluminosilicate glasses.

Keywords: Aluminosilicate glasses; Oxygen tri-clusters; Crack-resistance; Hardness

1. Introduction

Ideal structural materials for engineering applications should feature an optimized combination of tensile strength, hardness, toughness, elastic modulus, and damage resistance, but unfortunately such a combination is hard to be realized. Owing to their salient light transparency and relatively high thermal, mechanical, and chemical stabilities, oxide glasses promise wide applications in modern society, e.g., in touch panels, flexible electronics, photovoltaics, and batteries [1-4]. However, a significant drawback of oxide glasses is their brittleness, which makes them prone to catastrophic fracture under challenging conditions, thus limiting their applications as structural materials. To address this issue, it is crucial to discover ways to prevent crack initiation and curb their tendency to propagate.

Since the role of critical flaws in solid rupture was revealed by Griffith in 1921 [5], considerable efforts have been made to increase the resistance of glass to surface damage, e.g., by surface engineering [6,7]. Thermal tempering, ion exchange, and coatings are the predominant approaches for glass surface strengthening, which have resulted in remarkable commercial success. Despite the significance of these approaches, they have some limitations or drawbacks. For instance, when the elastic energy stored in glass during tempering is released upon external impact, catastrophic failure occurs in an explosive fashion, thus limiting their applications as structural materials. To overcome such problem, one of the effective strategies is to enhance the intrinsic crack resistance of glass by tuning its network structure through a rational design of material composition. In the past decade, many attempts have been devoted to lowering the brittleness of glasses, e.g., by tuning glass compositions based on the topological constraint theory [8,9] and the atomistic modeling [10]. Upon undergoing surface aging under humid conditions, cesium aluminoborate glasses displayed a record-

high crack initiation resistance of 500 N, which is about ten times greater than that of the annealed glass [11]. However, such glass system exhibits low chemical stability and relatively low hardness (2.0 GPa). Depending on its content in glass, the intermediate Al_2O_3 can act as network modifiers or formers. The positive role of Al_2O_3 in influencing the mechanical properties of glasses was manifested by the enhanced strength, hardness, and damage resistance, e.g., in commercial Corning Gorilla® glass series [12]. Nevertheless, the impact of increasing Al_2O_3 content on the crack resistance of oxide glasses still needs to be investigated.

By using the aerodynamic levitation and laser heating technique, we extended the glass-forming region of aluminosilicate glasses to $50CaO{\cdot}mAl_2O_3{\cdot}(100\text{-}m)SiO_2$ (m = 0~80), i.e., from pure silicate (m=0) to peraluminous composition (m=80). We detected the critical alumina fraction R (R is the molar ratio of [Al]/([Al]+[Si])), above which C_R starts to drastically rise with increasing R, indicating a brittle-to-ductile transition. To reveal the structural origin of this transition, by using a set of comprehensive strategies, we performed the Magic Angle Spinning (MAS) Nuclear Magnetic Resonance (NMR) experiments to characterize the short- and medium-range structure of the glass series. More importantly, for the first time to the best of our knowledge, we quantified the three coordinated oxygen fraction [$^{(3)}$O] from NMR data, and discovered that the increasing trend of [$^{(3)}$O] with R precisely follows that of C_R. This gives a strong implication that [$^{(3)}$O] is the main player in enhancing the C_R of aluminosilicate glasses.

2. Materials and Experimental Methods

2.1 Sample preparation

The calcium aluminosilicate glasses $50CaO{\cdot}mAl_2O_3{\cdot}(100\text{-}m)SiO_2$ (in molar fractions), where m

= 70,80 were prepared by a containerless aerodynamic levitation (ADL) laser-melting furnace built at Wuhan University of Technology [13,14], using 99.99% pure $CaCO_3$, Al_2O_3, SiO_2 powders (all from Aladdin) as raw materials. Prior to melting, precursors were heated at 800K in a muffle furnace for at least 2 hrs to remove adsorbed water. Then after weighed according to the stoichiometric ratio and mixed thoroughly using wet ball milling in ethanol for 2hrs, the batch was pressed into pellets with 20mm in diameter and 3mm in thickness at approximately 20MPa and sintered at 1373 K for 5 hrs. Specimens with a mass of approximately 18-25mg were taken from the pieces of broken pellets, placed in the conical nozzle of the ADL furnace. The sample was levitated by O_2 gas for avoiding SiO_2 volatilization, and melted completely at temperatures between 2000K and 2300K by CO_2 laser. The sample was kept in a molten state for about 10-20 s to ensure homogeneity. After turning off the laser, rapid cooling (~400°C/s) can be realized and glass beads with a diameter of ~2 mm was obtained.

In addition, the synthesized ^{17}O-enriched SiO_2 powders was used as one of the raw materials, the $50CaO$-mAl_2O_3-$(100-m)SiO_2$ glasses with m=80, 70, 65, 60, 50, and 40 were prepared by the ADL furnace according to the method mentioned above.

Finally, the $50CaO \cdot mAl_2O_3 \cdot (100-m)SiO_2$ glasses with m=65, 60, 50, 40, 20, and 0 were prepared by conventional melt-quenching method. Thoroughly mixed oxide powders (SiO_2, $CaCO_3$ and Al_2O_3) were melted using a Pt/Rh10 crucible in an electric furnace at about 1873 K for 3 hrs. Finally, the melts were poured onto a stainless steel plate in air, pressed using another stainless steel plate to obtain the homogeneous bulk glass, then annealed for 2 hrs at their respective annealing points (corresponding to $\eta=10^{12.3}$ Pa·s) to relieve the internal stress. The glassy nature of the samples was confirmed by featureless X-ray diffraction patterns and typical glass transition behaviors.

Based on the results of the X-ray fluorescence measurements, only minor discrepancy (±1 molar %) compared to their nominal compositions exists. Hereafter, the as-prepared glasses were given according to their nominal ones.

2.2 Synthesis of the ^{17}O-enriched SiO_2 powder

Applying the apparatus shown in Figure S1, ^{17}O-enriched SiO_2 powder was synthesized by using the isotopically enriched $H_2{}^{17}O$ (isotopic enrichment 95% from sigma) to hydrolyze $SiCl_4$ according to the following equation,

$$SiCl_4 + 2H_2{}^{17}O \xrightarrow{N_2} Si^{17}O_2 + 4HCl \quad (1)$$

We employed diethyl ether (Et_2O) as the dispersant agent to facilitate a smooth progression of the reaction with oxygen scrambling. N_2 as the protection gas prevents the H_2O from the air to affect the ^{17}O isotopic enrichment in the $Si^{17}O_2$ (Figure S1). To remove HCl, Et_2O and $SiCl_4$ remaining after the chemical reaction, the obtained powder was dried under vacuum at 500 K for 12 hrs, and then heat-treated at 1800 K in air for 5 hours.

2.3 Nuclear magnetic resonance (NMR) measurements

All the experiments were carried out at a Bruker Avance III HD 500 M spectrometer (11.7 T) with a 4 mm MAS probe. ^{17}O spin echo NMR spectra were recorded at a resonance frequency of 67.8 MHz at a spinning rate of 12 kHz. The 90° pulse length of 11 us and a relaxation time of 1 s were used. The ^{17}O chemical shift was referenced to H_2O (δ = 0 ppm). ^{27}Al MAS NMR spectra were record at a resonance frequency of 130.3 MHz. A spinning rate of 12 kHz, a liquid 15° pulse length of 1.1 μs and a relaxation time of 2.0 s were used. The ^{27}Al chemical shift was referenced to 1 M $Al(NO_3)_3$ solution (δ = 0 ppm). ^{29}Si MAS NMR spectra were acquired using the Hahn echo sequence at a

resonance frequency of 99.3 MHz, operating at a spinning rate of 6 kHz. The 90° pulse length of 6 μs and a relaxation time of 350 s were used. The ^{29}Si chemical shift was referenced to Tetrakis(trimethylsilyl)silane (δ = -9.7 ppm).

^{17}O{^{27}Al} double resonance signals were obtained using TRAPDOR pulse sequence [15], as shown in Figure 1. The spectra were collected at a spinning rate of 12 kHz. The pulse sequence involved a spin echo and central-transition selective 180° pulse on the ^{17}O channel in the absence (S_0) and presence (S) of a high-power recoupling pulse on the ^{27}Al channel. The 90° pulse length of 11 us and a relaxation time of 1 s were used on the ^{17}O channel. The TRAPDOR pulse was applied on the ^{27}Al channel only prior to the 180° ^{17}O echo pulse. The recoupling pulse power corresponds to a liquid nutation frequency of 16.67 kHz and the pulse length is 1.32 ms, corresponding to 16 integral rotor periods.

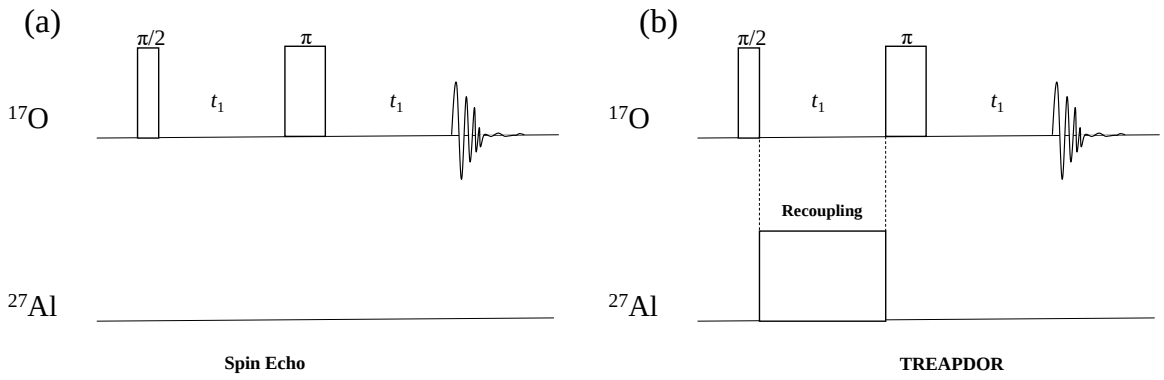

Figure 1. (a) Pulse schemes of ^{17}O Spin Echo and (b) ^{17}O{^{27}Al} TRAPDOR

A ^{27}Al{^{17}O} WURST-*J*-HMQC experiment was conducted at a spin rate of 12 kHz, using the pulse sequence illustrated in Figure 2 [16,17]. The ^{27}Al spin echo signal was increased by the WURST pulse and then modulated by two π/2 ^{17}O pulses. The mixing time τ for creating double quantum coherence via *J*-coupling was chosen to be 6 ms, during which the magnetization evolved. The length of two π/2 ^{17}O pulses applied on both sides of the ^{27}Al π pulse was 4.5 μs. The π/2 and π pulse lengths

of ^{27}Al were 7 μs and 14 μs, respectively. The double quantum coherence evolved during the interaction time t_1 that increased with a step of 41.67 μs (1/2 rotor period).

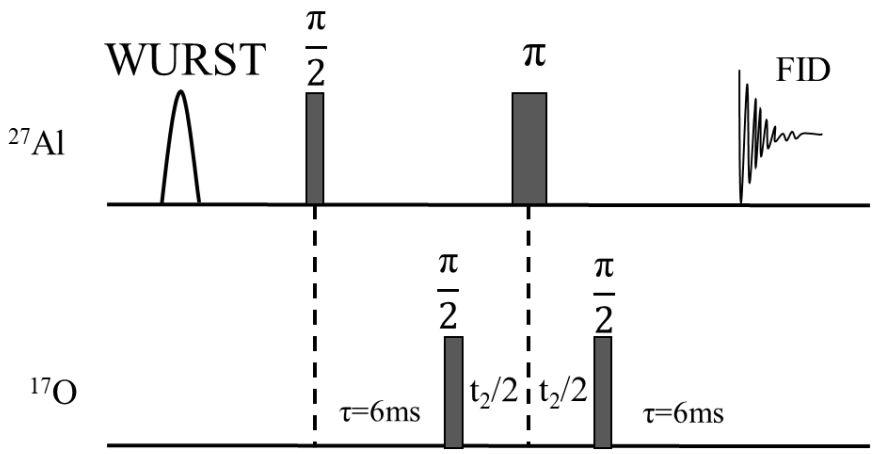

Figure 2. Pulse scheme of the 2D ^{27}Al{^{17}O} WURST-*J*-HMQC experiment.

^{27}Al triple-quantum magic angle spinning (TQMAS) NMR spectrum was collected at a frequency of 130.2 MHz using the three-pulse z-filtering pulse sequence (0.5 s recycle delay- 5.5 μs-τ_1(delay)-2.1 μs-echo delay-10 μs) [18,19] at a spinning speed of 12 kHz. The first two hard pulses and the third soft pulses correspond to liquid nutation frequencies of 57.47 kHz and 7.58 kHz, respectively. 360~972 scans per t1 increment were adopted depending on the Al content with a step of 10.42 μs. The sheared spectra were obtained by projecting each individual slice onto the F1 and F2 axes.

2.4 Micro-hardness and crack initiation resistance measurements

The measurements of Vickers hardness (H_V) were performed at room temperature and 55% relative humidity in air atmosphere using a micro-hardness Vickers tester (Q10A+, QNESS in

Austria). Mirror-polished glasses with approximately 500-μm thickness were used. Using an indentation time of 10 seconds and an indentation load of 0.98 N, 30 indents were conducted on each sample to obtain the mean value of H_V

To evaluate the crack initiation resistance (C_R) of a specimen, we generated thirty indents for each load with the series of loads. We counted, by means of optical microscopy, the number of corner cracks. Then, we calculated the probability of crack initiation by dividing the number of radial corner cracks with the number of total indent corners (four for each indent). We increased the indentation load step-by-step to ensure that the percentage of crack initiation increased from 0% to 100%. The percentage of crack initiation was plotted against the applied loads as shown in Figure S2. Following the definition of Wada [20], the load at which the probability arrives at 50% is determined as C_R.

2.5 Density measurements

The density ρ of the glasses was determined using helium ideal-gas pycnometry (ultrapyc 1200e, Quantachrome in American). The measurements were conducted 5 times for each sample.

2.6 Modulus Measurements

Young's Modulus and shear modulus of glass samples were determined by an ultrasonic measurement gauge. The ultrasonic wave velocities were recorded as longitudinal (V_L) and transverse wave (V_T). The velocities of sound wave propagated in the polished glass samples were measured using ultrasonic pulse-echo techniques (45MG, Olympus, USA). The test was performed using two transducers, one was M208 for longitudinal wave (10 MHz) and another was M110 for the transverse wave (5 MHz). Glycerin and burnt honey were used as bonding materials between samples and transducers. Elastic properties such as Young's modulus (E), shear modulus (G) and Poisson's ratio

(v) using the following standard equations:

$$Young's\ Modulus(E) = \frac{G(3\rho V_L^2 - 4G)}{(\rho V_L^2 - G)} \quad (2)$$

$$Shear\ Modulus(G) = V_T^2 \rho \quad (3)$$

$$\text{Possion's ratio}(v) = \frac{E}{2G} - 1 \quad (4)$$

where ρ is density and v is the Poisson's ratio of glass samples. Owing to the rather small size (about 2 mm) of the samples prepared by aerodynamic levitation furnace, we measured G, E, and υ only for the samples with R=0.46 to 0.79, since it was possible to produce large bulk samples by using the melt-casting techniques.

3. Results and Discussion

3.1 Mechanical performances

C_R, i.e., the critical indentation load, which is measured by Vickers indenter, is a generally used critical quantity to evaluate the ability of a glass to impede the crack initiation [21,22]. As shown in Figure 3a, the gradual substitution of Al for Si first causes a slight increase of C_R, i.e., from 0.9 N at R=0 to 5.1 N at R=0.67 in 50CaO·mAl$_2$O$_3$·(100-m)SiO$_2$ glasses. Then a sharp increase occurs in C_R by about 10 times, i.e., from 5.1 N at the critical R value of 0.67 to 45.6 N at R=0.89. The critical value R corresponds to the equal molar composition of Al$_2$O$_3$ and CaO. For the CaO-Al$_2$O$_3$ glasses, a critical point for C_R also appears at the equal molar composition of Al$_2$O$_3$ and CaO (Figure S3).

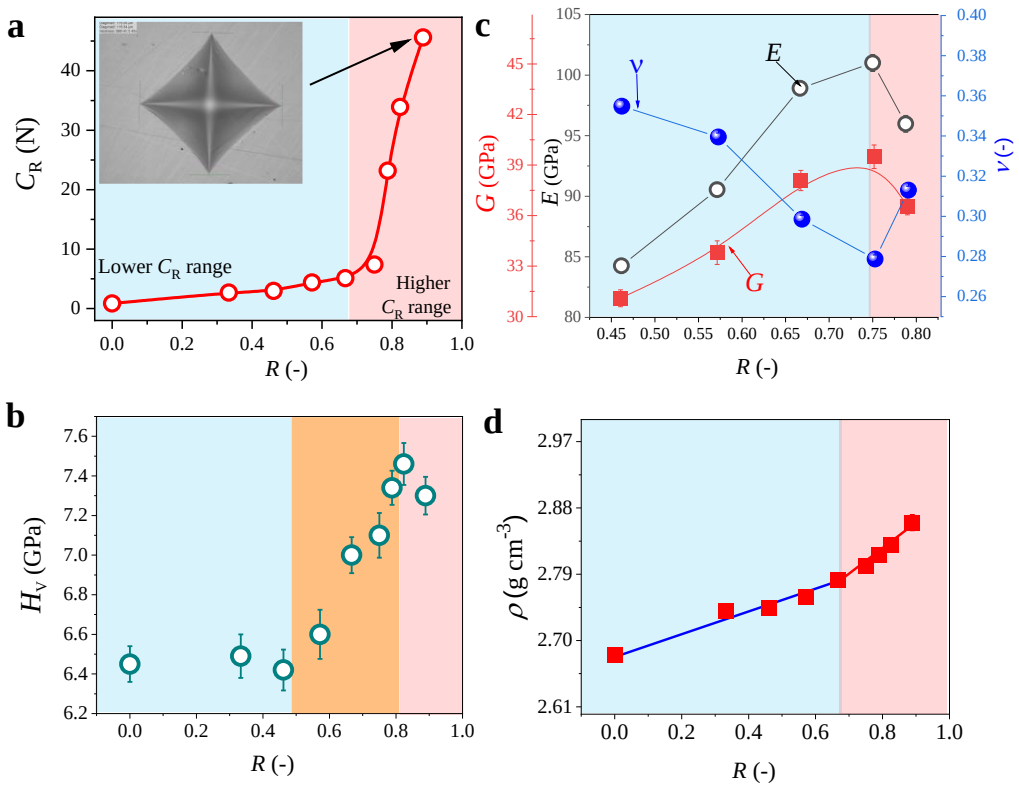

Figure 3. Alumina content dependence of mechanical properties for 50CaO·mAl$_2$O$_3$·(100-m)SiO$_2$ glasses. (a) Crack initiation resistance C_R; (b) Vickers microhardness H_V; (c) Shear modulus G, Elastic moduli E and Poisson's ratio υ; (d) Density ρ. Note: R=[Al/(Al+Si)]. The uncertainty of both E and G data is approximately ±0.2 GPa.

In addition, another evolutional mode in hardness (H_V) occurs (Figure 1b); i.e., two critical points appear. H_V remains constant (about 6.5 GPa) in the R range of 0.00 to 0.50. Then, H_V increases from 6.42 at R=0.5 to the maximum value of 7.46 GPa at R=0.82, followed by a drop at R=0.89. Interestingly, we also observe the maximum values of E (101 GPa) and G (39 GPa) and the minimum of υ (0.28) at R= 0.75 (Figure 3c).

3.2 Structural heterogeneity and calculation of $^{(3)}$O fraction

Structural heterogeneity is a striking feature of aluminosilicate glasses and exerts strong impact

on glass properties and functionalities. Structural heterogeneity refers to the scenario where a structure domain (e.g., a tetrahedra-ring in SiO_2) at medium-range scale (about 6~20Å) has a different atomic arrangement compared to its neighboring domains. For instance, one domain is rich in highly polymerized AlO_4 and SiO_4 units; while the other is rich in AlO_4, AlO_5, and AlO_6 units [23]. Till now, although the structural heterogeneity in aluminosilicate glasses was detected by several techniques [24-26], its content has not been experimentally determined yet. Particularly it seems impossible to quantify the fraction of the oxygen tri-clusters [$^{(3)}$O] from NMR techniques due to a high degree of overlap between the signals from the 2-coordinated bridging oxygen and those of the triply coordinated oxygen. In the following section, we characterize the detailed structure of the studied glass series and quantify the $^{(3)}$O fraction as a function of alumina by using our new NMR strategies.

Following Pauling's second rule (electrostatic valence balancing rule), when $[Al_2O_3]/[CaO]$ is equal to 1 (R=0.67), the glass structure should be completely composed of network forming tetrahedra, i.e., $[SiO_{4/2}]$ and $[AlO_{4/2}]^-$. The $[AlO_{4/2}]^-$ tetrahedra are charge compensated exactly by the amounts of Ca^{2+} at this ratio. By further adding Al_2O_3, triply or even higher coordinated oxygens should appear in the structural network. This is partly verified by the dominant and broad peak at about 49 ppm on the ^{17}O spectra of the ^{17}O enriched glasses (Figure 4a), which is ascribed to the bridging oxygens such as oxygen in Al-O-Al, Si-O-Al, Si-O-Si bonds, and triply or even higher coordinated oxygens [27]. The bridging oxygens in Al-O-Al and Si-O-Al linkages attract Ca^{2+} to compensate their negative charge, finally forming Al-O-(Al, Ca) and Si-O-(Al, Ca) bonds as shown in Figure S4. It is difficult to resolve the signals originated from various bridging oxygens and triply or even higher coordinated oxygens since they severely overlap with one another. With increasing the Al_2O_3 content, the signal

shifts toward higher chemical shift (Figure S5a), indicating that Si-O-(Al, Ca) bonds are increasingly replaced by Al-O-(Al, Ca) bonds.

However, a small fraction of non-bridging oxygens exists at the equivalent molar ratio of CaO and Al_2O_3 [23,27-29]. This is further confirmed by the weak signal at about 105 ppm on the ^{17}O spectra of the ^{17}O enriched $50CaO{\cdot}50Al_2O_3{\cdot}50SiO_2$ glass (Figure 4a), which is ascribed to the non-bridging oxygens. It should be noted that there are some debates concerning whether those non-bridging oxygens are connected with Si or with Al, or with both randomly [23,24,27-29].

By conducting the $^{17}O\{^{27}Al\}$ TRAPDOR and $^{27}Al\{^{17}O\}$ *J*-HMQC experiments, we further identify the connected neighbors of the non-bridging oxygens (NBOs); and find that these NBOs have great priority in bonding to Si, but not to Al. By using the pulse schemes of ^{17}O Spin Echo and $^{17}O\{^{27}Al\}$ TRAPDOR (Figure S6), we obtained the $^{17}O\{^{27}Al\}$ TRAPDOR spectra with and without the recoupling of $^{17}O \leftrightarrow {}^{27}Al$ dipolar-dipolar interaction, taking the $40Al_2O_3{\cdot}60SiO_2{\cdot}50CaO$ glass as an example, as presented in Figure 4b. Upon the recoupling of $^{17}O \leftrightarrow {}^{27}Al$ dipolar-dipolar interaction, the main peak shows evident attenuation while the weak one does not, implying that the bridging oxygen species should bond to Al^{3+} while the non-bridging oxygens should not. By further using the Pulse scheme of the $^{27}Al\{^{17}O\}$ WURST-HMQC experiment, the corresponding 2D $^{27}Al\{^{17}O\}$ *J*-HMQC spectrum was obtained as shown in Figure 4c, which reveals the strong correlation between the bridging oxygens and Al, but no signals from the corresponding nonbridging oxygens. This again confirms that the bridging oxygen species should be bonded to Al^{3+} while the non-bridging oxygen should not. Both results confirm that the non-bridging oxygens should bond to Si rather than to Al, despite the higher content of Al.

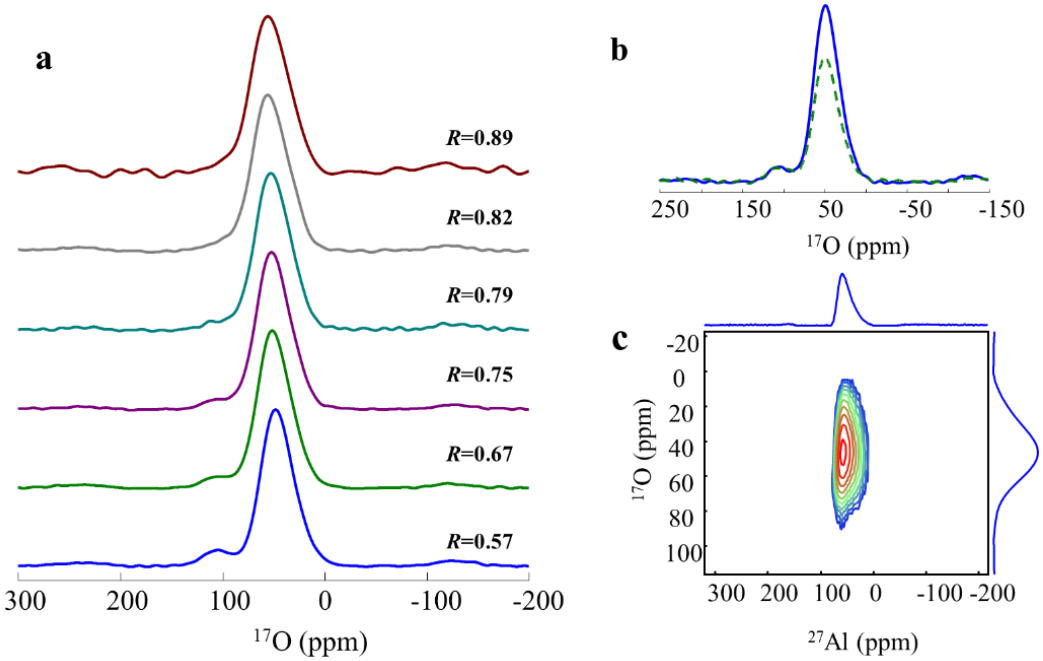

Figure 4. ^{17}O spectra of the ^{17}O enriched glasses. (a) ^{17}O spin echo spectra of $50CaO{\cdot}mAl_2O_3{\cdot}(100\text{-}m)SiO_2$ glasses. (b) $^{17}O\{^{27}Al\}$ TRAPDOR spectra of $40Al_2O_3{\cdot}60SiO_2{\cdot}50CaO$ glass. The green dashed and the blue solid lines represent the spectra with and without ^{27}Al excitation pulse, respectively. The excitation time is 1.32 ms. (c) 2D ^{27}Al $\{^{17}O\}$ WURST-*J*-HMQC spectrum of $40Al_2O_3{\cdot}60SiO_2{\cdot}50CaO$ glass.

The ^{27}Al spectra in Figures 5 and 6a also confirm that Al mainly exists in the form of Al(IV) ($[AlO_{4/2}]^-$ tetrahedra), together with a minor amount of Al(V, pentahedra) and even a tiny amount of Al(VI, octahedra). When *m* is smaller than 50, no Al(V) can be observed. To obtain high resolution signals, a typical ^{27}Al MQMAS spectrum is recorded (see Figure 6b), from which an intensive Al(IV) signal, a minor amount Al(V) and a weak Al(VI) signals are resolved, confirming the presence of Al(IV), Al(V) and Al(VI). A typical deconvolution of the ^{27}Al spectra for the glass with R=0.89 is shown in Figure 5. The deconvolution parameters of the glasses prepared with the enriched and the

natural abundance ^{17}O, respectively are listed in Table S3. Furthermore, the chemical shift of the Al(IV) increases with the increase of *m*, indicating the gradual change of the average local structure of Al(IV) with varying the composition.

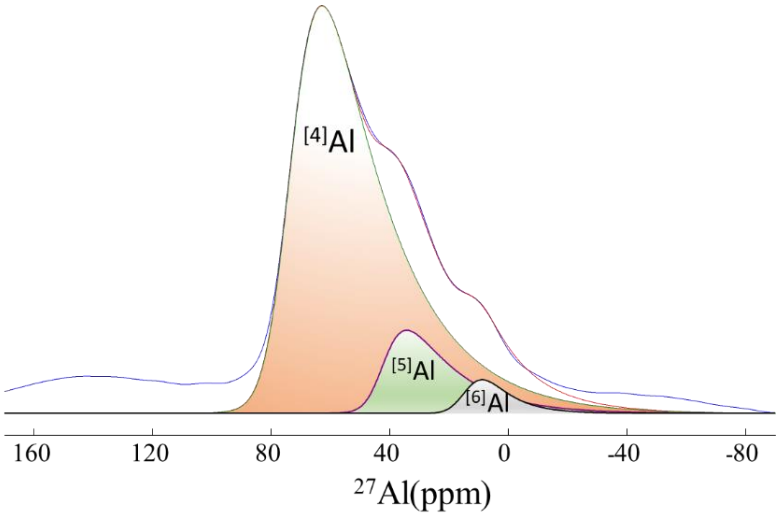

Figure 5. Deconvolution of the ^{27}Al spectra of the glass with the composition of $50CaO{\cdot}80Al_2O_3{\cdot}20SiO_2$ with enriched ^{17}O.

For the ^{29}Si spectra of the $50CaO{\cdot}mAl_2O_3{\cdot}(100\text{-}m)SiO_2$ glasses with R>0.67 (Figure 6c), according to the chemical shift [30], the broad peak at about -81.5 ppm should be ascribed to the Q^0_{4Al} species (Figure S4; n and i in Q^n_{iAl}, denote the numbers of Si-O bonds and Al-O bonds linking to each $[SiO_{4/2}]$, respectively). Q^0_{4Al} species is the $[SiO_{4/2}]$ tetrahedron bonded to four $[AlO_{4/2}]$ tetrahedra, each of which is charge-balanced by Ca^{2+}. According to Pauling's second rule, Si, Al and Ca contribute +1, +0.75 and +0.25 valence units to the oxygen, respectively. The average composition of the $Q^0_{(4Al)}$ species is $Ca_{0.5}AlSiO_4$. In this case, all the Si atoms will be firstly consumed to form the $Q^0_{(4Al)}$ species, which is confirmed by the stationary ^{29}Si spectral profile (Figure 6c). The similarity between the ^{27}Al and ^{29}Si spectra of the glasses prepared with enriched ^{17}O (Figures 6a and c) and those with natural abundance ^{17}O (Figures 7a and b) containing precursors suggests that the glass

structure depends only on the glass composition, not on the raw material. The surplus Al_2O_3 and CaO form clusters with the composition $Ca_xAl_yO_{(x+1.5y)}$, where y>2x. Thus, provided that the Al-avoidance rule can be strictly obeyed, the chemical reaction should be described as follows for the compositions with R>0.67:

$$m\mathrm{Al_2O_3}+(100-m)\mathrm{SiO_2}+50\mathrm{CaO} \Longrightarrow (100-m)\mathrm{Q^0_{(4Al)}}+ \mathrm{Ca_{m/2}Al_{(3m-100)}O_{(5m-150)}} \quad (5)$$

This equation clearly shows the inherent structural heterogeneity for these glasses. Only when the R value is higher than 0.67, three-coordinated oxygen clusters could be generated only in the $Ca_{m/2}Al_{(3m-100)}O_{(5m-150)}$ clusters. That is to say, the oxygen tri-cluster refers to the oxygen bonded by three Al atoms. Therefore, according to the Eq (1), the fraction of $^{(3)}O$ ($[^{(3)}O]$) in the total oxygen of these compositions with R>0.67 can be quantitatively calculated as follows:

$$[N_b]=([\text{Al-O}]- 4(100-m))/(5m-150) \quad (6)$$

$$[\text{Al-O}]=[Al^{IV}]\times4+[Al^{V}]\times5+[Al^{VI}]\times6 \quad (7)$$

$$[^{(3)}O]= ([N_b]-2)\times(5m-150)/(250+m) \quad (8)$$

where $[N_b]$ represents the average number of Al bonded to each O in $Ca_{m/2}Al_{(3m-100)}O_{(5m-150)}$ clusters, [Al-O] is the number of Al-O bonds, m represents the content of Al_2O_3, $[Al^{IV}]$, $[Al^{V}]$ and $[Al^{VI}]$ are the numbers of Al(IV), Al(V) and Al(VI), respectively, obtained from NMR spectra (Table S3). For detailed structural analysis, see Supporting Information.

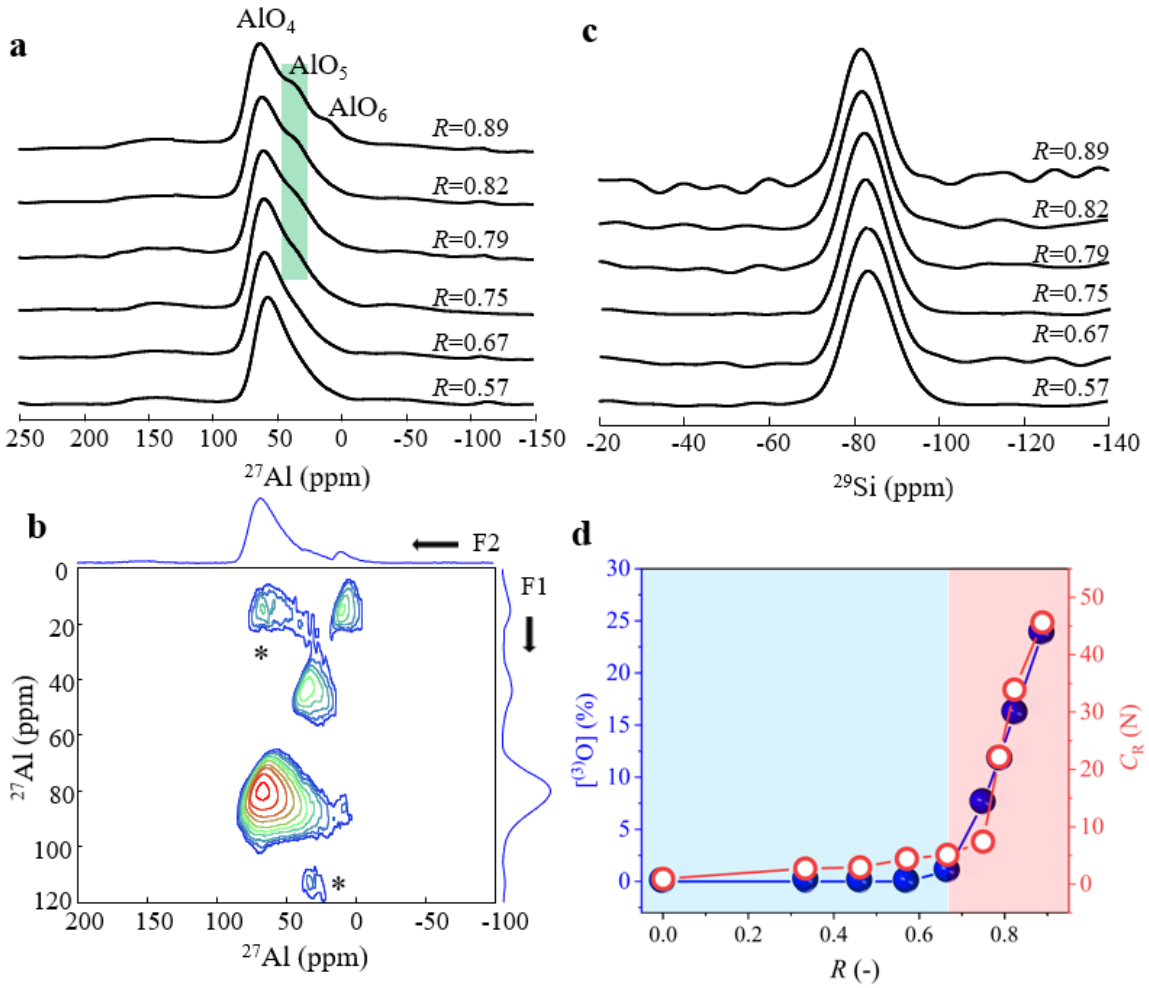

Figure 6. Structure characterizations by the Nuclear Magnetic Resonance Spectroscopy. (a) ^{27}Al spectra of 50CaO·mAl$_2$O$_3$·(100-m)SiO$_2$ glasses. (b) ^{27}Al MQMAS spectra of the glass with R=0.89, where the asterisks mark the spinning sidebands. (c) ^{29}Si spectra of ^{17}O enriched 50CaO·mAl$_2$O$_3$·(100-m)SiO$_2$ glasses with the molar ratio R=[Al/(Al+Si)]. (d) The comparison between the evolution trends of both [$^{(3)}$O] fraction and C_R with R.

3.3 Structural characteristics of high C_R glasses

To observe the cracking behavior of glass under mechanical impact, the sharp contact loading experiments are a simple and cost-effective way to evaluate the probability of crack initiation. Since the local displacement during densification is rather small, the stress produced by loading is dissipated

in glass, where the interatomic distances keep nearly constant and the corresponding bond angles change [11,31,32]. The densifying process leads to closer packing of atoms. Except densification, isochoric plastic flow could occur through bond switching, increasing or decreasing coordination numbers [33]. By stepwise increasing the load, the above-mentioned dissipating effect becomes rather small, and hence, cracks will initiate.

As mentioned above, some of Ca^{2+} ions can be network modifiers that cause NBOs and hence depolymerize the structural network. Therefore, the NBO-Ca^{2+} linkage is the weakest node in the glassy network upon external mechanical impact. In other words, the breakage of NBO-Ca^{2+} bonds could be the most possible origin of crack initiation, i.e., the reduced C_R. The NBO fraction decreases with increasing Al_2O_3 content, and therefore C_R rises from 0.9 to 5.1 N when m is increased from 0 to 50 in 50CaO·$m$$Al_2O_3$·(100-$m$)$SiO_2$ glass series.

A further addition of Al_2O_3 leads to a drastic enhancement in C_R for $m$$Al_2O_3$·(100-$m$)$SiO_2$·50CaO ternary glasses when the molar ratio of Al_2O_3/CaO is bigger than 1 (see Figure 3d). The structure network is constructed by the Q^0_{4Al} and $Ca_xAl_yO_{(x+1.5y)}$ clusters, where y>2x, as confirmed by NMR spectra. The similar enhancement in C_R is discovered in binary glasses with the composition (1-x)CaO·xAl_2O_3 (see Figure S3). This similarity indicates that the enhancement in C_R is associated with the role of the $Ca_xAl_yO_{(x+1.5y)}$ clusters. With increasing Al_2O_3 content, Figure 6d demonstrates a remarkable agreement between the evolution trend of C_R and that of the fraction of oxygen tri-clusters [$^{(3)}$O]. This gives a strong implication that the drastic C_R enhancement with R is attributed to the key role of $^{(3)}$O in preventing the crack initiation. The detailed explanation about the role of $^{(3)}$O is given below.

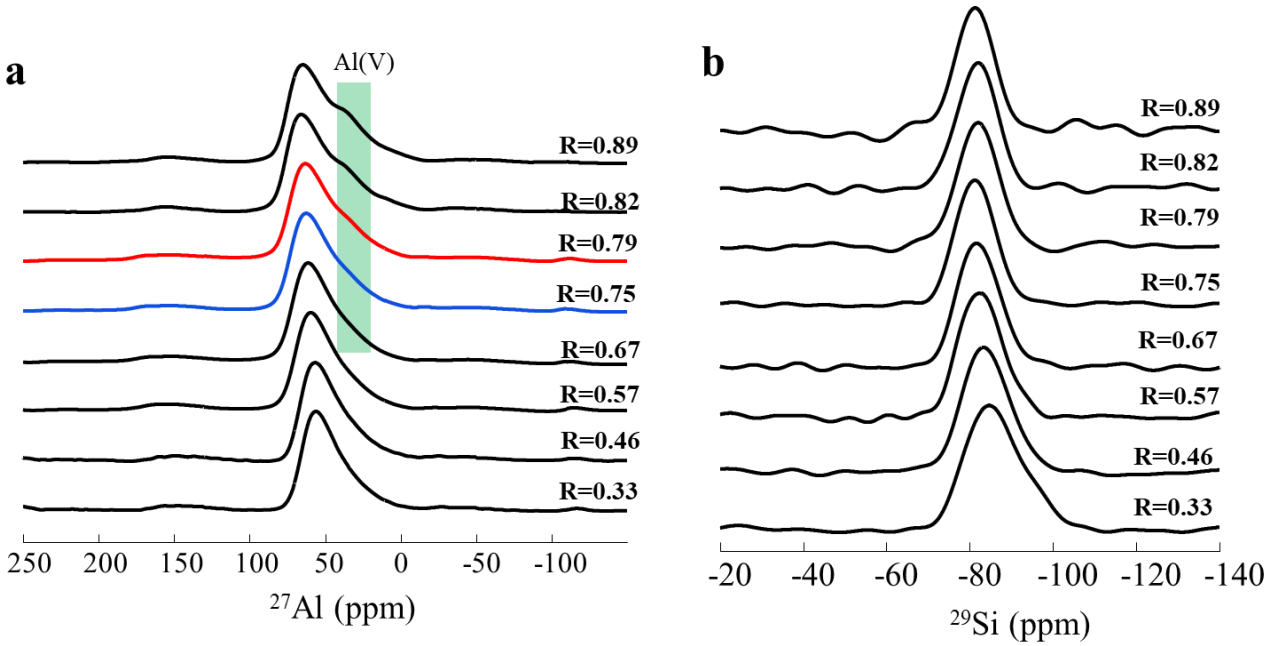

Figure 7. Structure characterizations by the Nuclear Magnetic Resonance Spectroscopy. (a) ^{27}Al spectra of $50CaO{\cdot}mAl_2O_3{\cdot}(100\text{-}m)SiO_2$ glasses with natural abundance ^{17}O. (b) ^{29}Si spectra of the investigated glasses prepared with natural abundance ^{17}O.

3.4 Role of oxygen tri-clusters in resisting crack initiation

Compared to the two-coordinated BOs, the bonds in oxygen tri-clusters are more ionic, weaker and more flexible [34]. Upon mechanical loading and unloading, these oxygen tri-clusters undergo an easier bond breaking-closing process. This process dissipates mechanical energy locally, and thus there will no sufficient energy to break the rigid bonds (BO-Si or BO-Al), hence preventing crack initiation and propagation. In other words, the oxygen tri-clusters can cause a certain degree of local ductility, and thereby making the glass tougher. The local ductility here refers to the mechanical state, where the structural building units undergo plastic deformation under stress before cracking. In this

study, it also means the short-range ductility, i.e., the ductility within the length scale of an oxygen tri-cluster (<6 Å). The microscopic mechanism of the effect of oxygen triclusters on C_R is schematically described by Figure 8. It is seen that the applied impact energy can be dissipated into glass network via oxygen tri-clusters, thereby avoiding the crack initiation and propagation. Route 1 illustrates the scenario where the coordinated oxygen number of the Al linked to $^{(3)}$O could be changed from 5 to 6 upon indentation. Route 2 displays the scenario where the Al-$^{(3)}$O bonds could be broken (bond opening) upon indentation and reconnected (bond re-closing). Route 3 refers to the case that the Al could be switched from one bridging oxygen to another, leading to the formation of another new $^{(3)}$O. Through these three routes, the external mechanical energy can be locally dissipated to prevent the initiation of microcracks. According to a prior study [35], the process of bond-breaking and reforming can induce network cavitation. This, in turn, leads to the nucleation of flaws, particularly on the surface of glass, ultimately reducing its crack resistance.

Furthermore, the $Ca_xAl_yO_{(x+1.5y)}$ phase is more prone to experiencing plastic flow or shear flow compared to the SiO_2-rich phase, owing to the fact that the average atomic bonding strength in the former is lower than that in the latter phase. As a result, the catastrophic breakage of rigid BO bonds can be averted. This is also the reason why, upon indentation, the glasses examined in this study display a noticeable pile-up, whereas pure silica glass does not demonstrate any pile-up. When the molar ratio (R) of [Al]/[Al+Si] surpasses the critical value of 67%, at which the oxygen triclusters fraction starts to increase, both crack initiation and propagation in the glass during indentation are significantly suppressed. This suppressing effect becomes stronger with increasing the fraction of oxygen tri-clusters (R) when [Al] content exceeds the critical content that corresponds to the R value

of 0.67 (Figure 6d).

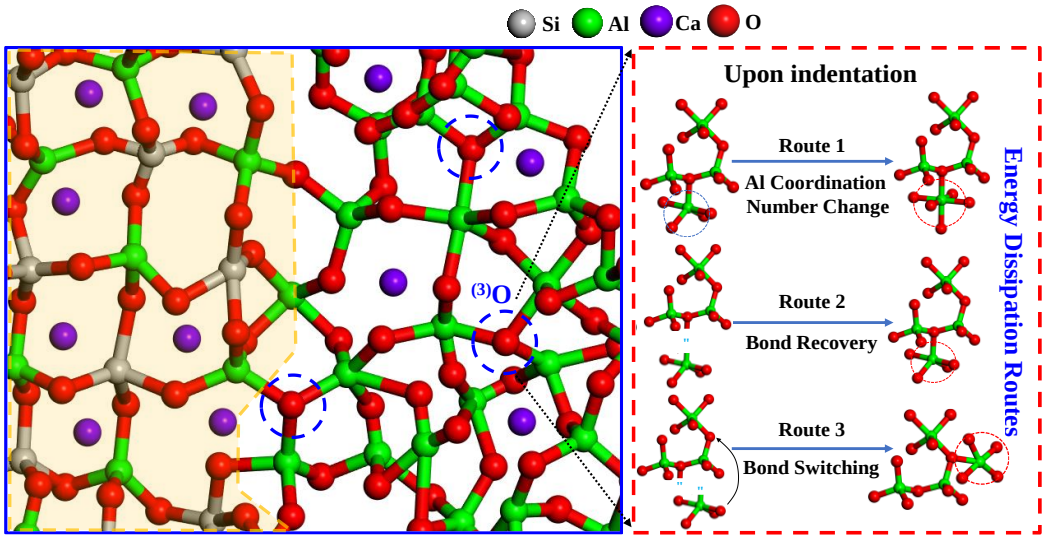

Figure 8. Schematic diagrams of microscopic mechanism for the drastic enhancement of crack initiation resistance. Left panel: Illustration of structural heterogeneity in intermediate-range scale for the calcium aluminosilicate glasses with [Al]/([Al]+[Si])>~0.7. The structural heterogeneity involves two types of clusters: $Ca_{0.5}AlSiO_4$ cluster (yellow shaded area) and the Al_2O_3-rich $Ca_{m/2}Al_{(3m-100)}O_{(5m-150)}$ cluster that contains the oxygens ($^{(3)}$O) coordinated to three AlO_x polyhedra (highlighted by the blue dashed circles). Right panel: Illustration of the indentation energy dissipation into local structure to prevent the crack initiation. The energy dissipation is realized through three possible routes of the change of the bonding environment of $^{(3)}$O. *Route 1*: change of the coordination number of Al from 5 to 6 ; *Route 2*: opening and reclosing of $^{(3)}$O-Al bonds; *Route 3*: switching of one $^{(3)}$O-Al bond to another bridging oxygen.

As an indicator of deforming ability for a material, H_V can reach at a same value through different ways such as densification or volume-conserved plastic flow [36]. Note that the deformation of glass during indentation involves the three processes: elastic deformation, densification, and plastic flow [37]. The H_V value of glass serves as a measure of its overall resistance to deformation. It is

anticipated that densification plays a key role on H_V in the low-C_g glasses, whereas the plastic flow is predominant in the high C_g glasses. The plastic flow caused by indentation is a kind of shear flow that leads to the formation of pile-up [38]. This shear is associated with the translational motion of structural units [39]. H_V is the result of a competition between the bond strength and C_g.

By increasing the fraction of oxygen triclusters in the aluminosilicate glass system, we have observed a synergistic effect on its mechanical properties. Specifically, the glass not only becomes more resistant to crack initiation but also harder. However, this synergistic effect cannot be achieved for boroaluminosilicate glasses. The potential reason for the disparity between the two glass systems may be as follows. In contrast to boroaluminosilicate glasses, these aluminosilicate glasses with $R > 0.67$ demonstrates the following characteristics: (1) a high fraction of oxygen triclusters; and (2) lower densification but greater elastic volume recovery. The former contributes to high crack resistance, whereas the latter leads to increased hardness.

As shown in Figure 3b, a distinct drop in H_V above R=0.82 occurs since the plastic flow becomes more predoiminant compared with densification. Additionally, H_V also shows a certain decrease at R=0.82, which corresponds to an increase in plastic deformation. The easier plastic flow might originate from the increase in AlO_5 pentahedra and oxygen triclusters.

E and G can be regarded as an indirect measure of the mean bond energy density per unit volume. They reach the maximum values at R=0.75, i.e., at lower R value, compared to the case of H_V maximum at R=0.82. The hardness and modulus are usually positively correlated with the dissociation energy per unit volume in a glass. Taking into account the influence of both average bond strength and C_g on H_V, it can be asserted that atomic packing density predominantly contributes to H_V

enhancement. Lastly, Poisson's ratio (υ), defined as the ratio of lateral strain to longitudinal strain, reaches a minimum value (~0.28) at R=0.75. The minimum υ value is slightly higher than those of most brittle inorganic glasses [40]. As reported in [41], the elastic volume recovery non-linearly increases with a decrease of the υ value. Thus, it can be inferred that the degree of the elastic volume recovery in our glasses must increase with increasing the R value from 0.67 to about 0.75, because Poisson's ratio decreases with R in this range (Fig. 3c). More elastic recovery implies that the glass can undergo a higher degree of elastic deformation during indentation, resulting in higher hardness. However, the Poisson's ratio abnormally increases as R increases from around 0.75 to 0.8, whereas both E and G moduli drop (Fig. 3c). Contrastingly, the glass hardness experiences an abnormal decrease when R rises from around 0.8 to 0.9 (Fig. 3b). This means that the R value (approximately 0.75) marking the onset of the decrease in E, G and the increase in υ differs from the value (around 0.8) associated with the increase in H_V.

The crack resistance of glasses depends not only on glass structure, but also on contact geometry. A previous study showed that an increase in indenter sharpness, indicated by a lower tip angle, leads to a reduction in crack resistance [42]. Likewise, another study illustrated that a sharper indenter typically led to a narrower transition region between areas where no cracks were initiated and areas where full crack initiation occurred [43]. It is important to emphasize that the improvement in crack resistance due to an increase in the oxygen tricluster fraction was assessed solely in this work using an indenter with a tip angle of 136 degrees.

The C_R value exhibits a significant increase of about tenfold as R was raised from 0.67 to 0.89. Nonetheless, had a smaller tip angle indenter been employed, it is anticipated that the increase in

crack resistance would have been diminished [42,43]. There may still be some level of improvement in crack resistance (C_R) when using the sharper indenter, as structural factors like oxygen triclusters are expected to have a positive impact. In any case, utilizing indenters with smaller tip angles will be important for future studies to validate the practical significance of the present work. The crack resistance of these glasses should be evaluated under conditions that mimic their real-world applications, where sharper indenting or sharper edge impact may be encountered.

4.Conclusions

We observed that the crack resistance (C_R) of calcium aluminosilicate glasses sharply rises with increasing the molar ratio of [Al]/[Al+Si] when this ratio exceeds the critical value 0.67. The occurrence of the triply coordinated oxygens (i.e., the oxygen tri-clusters) is the key to enhance C_R value and to make the glass mechanically more robust. We deemed that the role of the oxygen tri-clusters in enhancing C_R is associated with the scenario where these clusters may dissipate the external mechanical impacting energy via more frequent bond-open-reclosing events compared with the 2-coordinated bridging oxygens. The local energy dissipation increases the local ductility and thereby lowers the probability of the breakage of rigid bridging oxygen bonds, consequently mitigating the crack initiation and propagation.

Acknowledgments

This work was financially supported by National Natural Science Foundation of China (No. 52172007), plan to boost the project of innovative talents by Ministry of Science and technology of the people's republic of China (No.2017RA4038), and Key R&D projects in Hubei Province (2022BAA025).

Conflict of interest: The authors declare no competing financial interests.

Data availability: The data that support the findings of this study are available from the corresponding author upon reasonable request.

References

[1] E. J. Frankberg, J. Kalikka, F. García Ferré, L. Joly-Pottuz, T. Salminen, J. Hintikka, M. Hokka, S. Koneti, T. Douillard, B. Le Saint, Highly ductile amorphous oxide at room temperature and high strain rate, Science 366 (2019) 864–869.

[2] Y. Idota, T. Kubota, A. Matsufuji, Y. Maekawa, T. Miyasaka, Tin-based amorphous oxide: a high-capacity lithium-ion-storage material, Science 276 (1997) 1395–1397.

[3] X. Yu, T. J. Marks, A. Facchetti, A. Metal oxides for optoelectronic applications, Nat. Mater. 15 (2016) 383–396.

[4] K. Nomura, H. Ohta, A. Takagi, T. Kamiya, M. Hirano, H. Hosono, Room-temperature fabrication of transparent flexible thin-film transistors using amorphous oxide semiconductors, Nature 432 (2004) 488–492.

[5] A. A. Griffith, VI. The phenomena of rupture and flow in solids, Philosophical transactions of the royal society of london. Series A, containing papers of a mathematical or physical character 221 (1921) 163–198.

[6] G. Sani, R. Limbach, J. Dellith, İ. Sökmen, L. Wondraczek, Surface damage resistance and

yielding of chemically strengthened silicate glasses: From normal indentation to scratch loading, J. Am. Ceram. Soc. 104 (2021) 3167–3186.

[7] K. S. R. Karlsson, L. Wondraczek, Strengthening of oxide glasses, Encyclopedia of Glass Science, Technology, History, and Culture 1 (2021) 391–404.

[8] M. M. Smedskjaer, J. C. Mauro, Y. Yue, Prediction of glass hardness using temperature-dependent constraint theory, Phys. Rev. Lett. 105 (2010) 115503.

[9] M. M. Smedskjaer, J. C. Mauro, S. Sen, Y. Yue, Quantitative design of glassy materials using temperature-dependent constraint theory, Chem. Mater. 22 (2010) 5358–5365.

[10] J. C. Mauro, A. Tandia, K. D. Vargheese, Y. Yue, M. M. Smedskjaer, Accelerating the Design of Functional Glasses through Modeling, Chem. Mater. 28 (2016) 4267–4277.

[11] K. Januchta, M. Stepniewska, L. R. Jensen, Y. Zhang, M. A. Somers, M. Bauchy, Y. Yue, M. M. Smedskjaer, Breaking the limit of micro-ductility in oxide glasses, Adv. Sci. 6 (2019) 1901281.

[12] C. Ragoen, S. Sen, T. Lambricht, S. Godet, Effect of Al_2O_3 content on the mechanical and interdiffusional properties of ion-exchanged Na-aluminosilicate glasses, J. Non-Cryst. Solids 458 (2017) 129–136.

[13] Z. Shan, S. Liu, H. Tao, Y. Yue, Mixed alkaline-earth effects on several mechanical and thermophysical properties of aluminate glasses and melts, J. Am. Ceram. Soc. 102 (2019) 1128–1136.

[14] X. Ke, Z. Shan, Z. Li, Y. Tao, Y. Yue, H. Tao, Toward hard and highly crack resistant magnesium aluminosilicate glasses and transparent glass-ceramics, J. Am. Ceram. Soc. 103 (2020) 3600–3609.

[15] C. P. Grey, A. J. Vega, Determination of the Quadrupole Coupling Constant of the Invisible Aluminum Spins in Zeolite HY with $^{1}H/^{27}Al$ TRAPDOR NMR, J. Am. Chem. Soc. 117 (1995) 8232–

8242.

[16] A. Lesage, D. Sakellariou, S. Steuernagel, L. Emsley, Carbon−Proton Chemical Shift Correlation in Solid-State NMR by Through-Bond Multiple-Quantum Spectroscopy, J. Am. Ceram. Soc. 120 (1998) 13194–13201.

[17] Q. Wang, J. Trébosc, Y. Li, J. Xu, B. Hu, N. Feng, Q. Chen, O. Lafon, J.-P. Amoureux, F. Deng, Signal enhancement of J-HMQC experiments in solid-state NMR involving half-integer quadrupolar nuclei, Chem. Commun. 49 (2013) 6653–6655.

[18] J.-P. Amoureux, C. Fernandez, S. Steuernagel, ZFiltering in MQMAS NMR, J. Magn. Reson. 123 (1996) 116–118.

[19] A. Medek, J. S. Harwood, L. Frydman, Multiple-Quantum Magic-Angle Spinning NMR: A New Method for the Study of Quadrupolar Nuclei in Solids, J. Am. Chem. Soc. 117 (1995) 12779–12787.

[20] M. Wada, H. Furukawa, K. Fujita, Crack resistance of glass on Vickers indentation, Proc. Xth Int. Congr. Glas. 11 (1974) 39–46.

[21]C. Moysan, R. Riedel, R. Harshe, T. Rouxel, F. Augereau, Mechanical characterization of a polysiloxane-derived SiOC glass, J. Eur. Ceram. Soc. 27 (2007) 397–403.

[22]C. Hermansen, J. Matsuoka, S. Yoshida, H. Yamazaki, Y. Kato, Y. Z. Yue, Densification and plastic deformation under microindentation in dilicate glasses and the relation to hardness and crack resistance. J. Non-Cryst. Solids 364 (2013) 40-43.

[23]D. R. Neuville, L. Cormier, D. Massiot, Al coordination and speciation in calcium aluminosilicate glasses: Effects of composition determined by ^{27}Al MQ-MAS NMR and Raman spectroscopy, Chem. Geol. 229 (2006) 173–185.

[24] M. Moesgaard, R. Keding, J. Skibsted, Y. Yue, Evidence of intermediate-range order heterogeneity in calcium aluminosilicate glasses, Chem. Mater. 22 (2010) 4471–4483.

[25] Y. Yue, C. A. Angell, Clarifying the glass-transition behaviour of water by comparison with hyperquenched inorganic glasses, Nature 427 (2004) 717–720.

[26] Y. Yue, Revealing the nature of glass by the hyperquenching-annealing-calorimetry approach, J. Non-Cryst. Solids: X. 14 (2022) 100099.

[27] J. F. Stebbins, J. V. Oglesby, S. Kroeker, Oxygen triclusters in crystalline $CaAl_4O_7$ (grossite) and in calcium aluminosilicate glasses: ^{17}O NMR, Am. Mineral. 86 (2001) 1307–1311.

[28] L. M. Thompson, J. F. Stebbins, Non-stoichiometric non-bridging oxygens and five-coordinated aluminum in alkaline earth aluminosilicate glasses: Effect of modifier cation size, J. Non-Cryst. Solids 358 (2012) 1783–1789.

[29] L. M. Thompson, J. F. Stebbins, Non-bridging oxygen and high-coordinated aluminum in metaluminous and peraluminous calcium and potassium aluminosilicate glasses: High-resolution ^{17}O and ^{27}Al MAS NMR results. Am. Mineral. 96 (2011) 841–853.

[30] J. F. Stebbins, Z. Xu, NMR evidence for excess non-bridging oxygen in an aluminosilicate glass, Nature 390 (1997) 60–62.

[31] J. Sehgal, S. Ito, A new low-brittleness glass in the soda-lime-silica glass family, J. Am. Ceram. Soc. 81 (1998) 2485–2488.

[32] H. Morozumi, S. Yoshida, J. Matsuoka, Composition dependence of crack formation probability in aluminoborosilicate glass, J. Non-Cryst. Solids 444 (2016) 31–37.

[33] T. To, S. S. Sørensen, J. F. Christensen, R. Christensen, L. R. Jensen, M. Bockowski, M. Bauchy,

M. M. Smedskjaer, Bond switching in densified oxide glass enables record-high fracture toughness, ACS Appl. Mater. Interfaces 13 (2021) 17753–17765.

[34] A. V. Nemukhin, F. Weinhold, Structures of the aluminum oxides studied by ab initio methods with natural bond orbital analysis, J. Chem. Phys. 97 (1992) 3420–3430.

[35] S. Ito, T. Taniguchi, Effect of cooling rate on structure and mechanical behavior of glass by MD simulation, J. Non-Cryst. Solids 349 (2004) 173-179.

[36] T. Rouxel, J. Jang, U. Ramamurty, Indentation of glasses, Prog. Mater. Sci. 121 (2021) 100834.

[37] M. Yamane, J.D. Mackenzie, Vicker's Hardness of glass, J. Non Cryst. Solids 15 (1974) 153-164.

[38] J. Kjeldsen, M.M. Smedskjaer, J.C. Mauro, Y. Yue, Hardness and incipient plasticity in silicate glasses: Origin of the mixed modifier effect, Appl. Phys. Lett. 104 (2014) 051913.

[39] J. Kjeldsen, M.M. Smedskjaer, J.C. Mauro, R.E. Youngman, L. Huang, Y. Yue, Mixed alkaline earth effect in sodium aluminosilicate glasses, J. Non-Cryst. Solids 369 (2013) 61-68.

[40] M. B. Østergaard, S. R. Hansen, K. Januchta, T. To, S. J. Rzoska, M. Bockowski, M. Bauchy, M. M. Smedskjaer, Revisiting the dependence of poisson's ratio on liquid fragility and atomic packing density in oxide glasses, Materials 12 (2019) 2439.

[41] S. Yoshida, J.C. Sanglebœuf, T. Rouxel, Quantitative evaluation of indentation-induced densification in glass, J. Mater. Res. 20 (2005) 3404-3412.

[42] T.M. Gross, Deformation and cracking behavior of glasses indented with diamond tips of various sharpness, J. Non-Cryst. Solids 358 (2012) 3445-3452.

[43] J.F.S. Christensen, N.M.A. Krishnan, M. Bauchy, M.M. Smedskjaer, Indenting glasses with indenters of varying stiffness and sharpness, J. Non-Cryst. Solids 603 (2023) 122111.